UDC 551.513.1:551.587(213)

Remote Forcing of the Time-Independent Tropical Atmosphere

PETER J. WEBSTER [1]—*Commonwealth Meteorology Research Centre, Melbourne, Australia*

ABSTRACT—An analysis is made of low-latitude, large-scale, zonally asymmetric motions that result from the influence of stationary extratropical disturbances. A linear, two-layer, primitive-equation model in spherical coordinates with parameterized dissipation and realistic basic flows is used. Midlatitude effects are included by applying conditions at the lateral boundaries of the model near 40°N and 40°S.

A series of hypothetical cases is considered in which the roles of dissipation and various basic fields are studied for their effect on the equatorward propagation of energy. The interaction of seasonal forcing functions and basic states in December, January, and February and in June, July, and August is studied. The response near the Equator is found to depend on both the basic state and the magnitude of the forcing, although generally the midlatitude effects dominate the subtropics, whereas local forcing is of greater importance in low latitudes.

A comparison of the computed composite state of the tropical atmosphere (due to both local and remote forcing) with observed fields and previous studies indicates a successful simulation of many features of the seasonal mean tropical atmosphere.

1. INTRODUCTION

In a recent study, Webster (1972) (hereafter referred to as W1) investigated theoretically the dynamics of low-latitude, large-scale, zonally asymmetric motions driven by forcing functions located within equatorial regions. Latent heating was found to be the most important *local* forcing function, although the importance of orography increased to near parity with it in the subtropics. Between 20°N and 20°S, the calculated seasonal response appeared to agree with observations, although poleward of these latitudes large discrepancies were found in specific regions, especially in the North Pacific Ocean. These differences in the subtropical regions were believed to occur as a result of the influence of extratropical forcing, which had been purposely omitted from W1. It is the purpose of this study to investigate the influence of the steady-state circulation of the midlatitudes upon the steady-state low latitudes.

The existence of time-independent modes in midlatitudes has been the subject of many studies dating back to the work of Rossby and colleagues (Rossby 1939), who investigated the quasi-permanent location of certain large-scale features in the westerlies. Eliassen and Palm (1961) suggested that such circulations could yield an important effect on the low-latitude flow. They showed that in a westerly regime the wave energy flux of stationary modes is in an opposite sense to the momentum flux and is, therefore, equatorward. Their study indicated that penetration of wave energy to lower latitudes is a strong function of the form of the basic flow.

During the last few years, a considerable amount of work has been done concerning the interaction of propagating waves and shear flow (e.g., Booker and Bretherton 1967, Jones 1967, Charney 1969, Dickinson 1970, and many others). Two papers (Mak 1969, Bennett and Young 1971) are of particular relevance to our study; both consider the interaction of midlatitudes and the Tropics by imposed conditions on the lateral boundaries of an equatorial channel. The former study used a model similar to that considered in the present study, whereas Bennett and Young used a simpler, shallow fluid model with only horizontal shear. Both studies dealt particularly with transient modes. Mak (1969) forced his Tropics over a wide range of frequencies, using observed data as input at the two boundaries (actually, due to the Southern Hemisphere data problem, Mak assumed identical condition at both boundaries), whereas Bennett and Young (1971) used simpler boundary conditions to analyze the physics of Mak's results. Specifically, they were interested in the selective filtering of the various modes of the system by the basic field. Both studies used analytic basic fields that are similar in form to that used in case T1 (table 1) in Mak's study and case T2 in Bennett and Young's study.

The principal results obtained by Bennett and Young (1971) defined the selectiveness of the basic field and are generally consistent with the results obtained by the physical arguments of Charney (1969). To summarize, waves with phase speeds somewhere equal to that of the basic flow at some latitude, μ_c (the "critical latitude" [2]), are absorbed by the mean flow at that latitude. These are the Rossby modes of cyclone scale. Larger scale Rossby waves with phase speeds greater than the basic flow anywhere are permitted to propagate into the Tropics. Similarly, the rapidly moving eastward- and

[1] Now at the Department of Meteorology, University of California, Los Angeles.

[2] The critical latitude, μ_c, is that latitude where the Doppler-shifted frequency (i.e., the frequency of the mode relative to the rotating observer) is zero. For example, a Rossby wave that has a negative phase speed will possess a critical latitude somewhere within the easterly wind regime.

TABLE 1.—*Definition of the various hypothetical cases.* A_i *is the amplitude of the boundary condition [eq (7)], and* $\bar{U}_i$ *defines the form of the basic state within the equatorial channel.*

Case	Amplitude A_i m/s				$\bar{U}_i(\mu,p)$ m/s	
	$\mu=-0.6$		$\mu=0.6$			
	250 mb	750 mb	250 mb	750 mb	250 mb	750 mb
T1	−5	−5	0	0	$\bar{U}_1=18\sin\frac{3\pi}{2}(\mu+1)+14(1-\mu^2)$	$\bar{U}_2=7\sin\frac{3\pi}{2}(\mu+1)+2(1-\mu^2)$
T2	−5	−5	0	0	$\bar{U}_1=12.5\sin\frac{3\pi}{2}(\mu+1)+8(1-\mu^2)$	$\bar{U}_2=\bar{U}_1$
T3	−5	−5	0	0	$\bar{U}_1=5$ m/s	$\bar{U}_2=\bar{U}_1$
T4	−5	−5	0	0	$\bar{U}_1=-5$ m/s	$\bar{U}_2=\bar{U}_1$

westward-propagating gravity waves are also able to influence the low latitudes.

In the next section, an outline of the model will be presented; in section 3, the lateral boundary conditions are formulated. In section 4, a series of hypothetical basic states will be excited by a specific form of the forcing function at the southern boundary of the model to study the equatorial propagation of wave energy in a dissipative system with shear. In this section, we will also calculate the response of the December, January, and February (DJF) and the June, July, and August (JJA) basic states to the appropriate forcing at the lateral boundaries. In section 5, we will compare the response of low latitudes to local and remote forcing and finally compare the total response (due to both local and remote forcing) with the observed seasonal state of the tropical atmosphere.

2. THE MODEL TROPICS

To facilitate the study of the response of the Tropics to midlatitude forcing, we will use a model similar to one formulated in W1. Only the domain of the model will be changed. In the study of *local* steady forcing of the Tropics (W1), no constraint was placed on the latitudinal extent of the model. However, in this investigation, we are compelled to restrict the poleward limits of the Tropics by walls at arbitrary latitudes and to treat the behavior of the atmosphere poleward of these boundaries in terms of known spatial functions. The manner in which the midlatitudes and the tropical regime interact is thus governed by the latitudinal boundary conditions. With the influence of the midlatitudes included in the above manner and the neglect of all forcing from within the Tropics, the model reduces to one used by Mak (1969) for the study of time-dependent transient motions.

Since a detailed derivation of the governing equations of the model is given in W1, only a brief outline will be presented here. The basic field, which we will perturb, is one that is consistent with a known basic zonal flow,

$$\bar{U}(\mu,p)=(1-\mu^2)^{1/2}(2\Omega a)\Delta(\mu,p), \tag{1}$$

where a and $1/2\Omega$ represent the earth's radius and period of rotation, respectively, $\Delta(\mu, p)$ is some nondimensional function, and μ and p represent the sine of latitude and the pressure, respectively. The overbar denotes a zonal average. Without orography or heating effects, the spherical equations of motion, linearized about eq (1), may be written as

$$\Delta u_\varphi+(1-\mu^2)v\Delta_\mu+(1-\mu^2)\Delta_p-\mu v(2\Delta+1) =-\psi_\varphi+(1-\mu^2)^{1/2}F_\varphi, \tag{2a}$$

$$\Delta v_\varphi+\mu v(2\Delta+1)=-(1-\mu^2)\psi_\mu+(1-\mu^2)^{1/2}F_\mu, \tag{2b}$$

$$u_\varphi+(1-\mu^2)(\omega_p+v_\mu)=0, \tag{2c}$$

$$\Delta(\psi_p)_\varphi+v(\bar{\Psi}_p)_\mu+\frac{\omega\bar{S}(p)}{p^2}=\frac{\dot{Q}}{p}, \tag{2d}$$

and

$$\bar{\Psi}_\mu=-\Delta(1+\Delta)\mu. \tag{2e}$$

The above equations have been nondimensionalized using $1/2\Omega$, a, and $p_0(=1000$ mb) as time, length, and pressure scales, respectively. The terms u, v, and ω are the zonal, meridional, and vertical components [multiplied by $(1-\mu^2)^{1/2}$] of the velocity vector, $\bar{\Psi}$ and ψ represent the mean and perturbation parts of the geopotential field, and φ is longitude. Simple linear dissipation mechanisms have been included in the above equations via F_φ, F_μ, and $\dot{Q}$. These include a radiational cooling term, a surface drag effect, and a representation of the small-scale exchange of momentum in the vertical (see W1 for further details). Throughout this study, the values of the dissipation coefficients are the same as those used in the earlier study inferring decay rates of 6, 25, and 40 days, respectively. Similarly, the stability function, $\bar{S}$, has the value of 0.0083.

Applying the conditions that

$$\omega(p=0)=\omega(p=1)=0, \tag{3}$$

we express the governing equations in the two-layer system shown schematically in figure 1. The dependent variables of the system are u_i, v_i, ψ_i, and ω. The subscript $i=1$ denotes the upper level (250 mb) and 2, the lower level (750 mb). The symbol ω represents the vertical velocity at 500 mb.

The longitudinal variation is separated out by expanding the variables in a Fourier series in φ. For example,

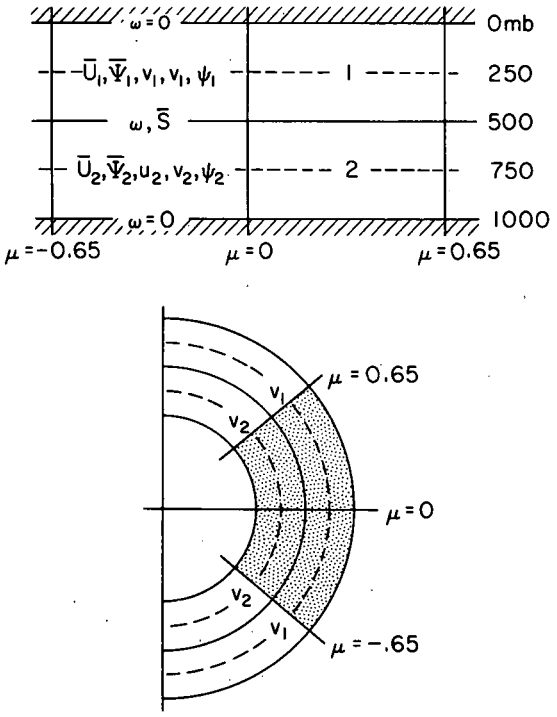

FIGURE 1.—Schematic representation of the two-layer spherical model with lateral boundaries near 40°N and 40°S.

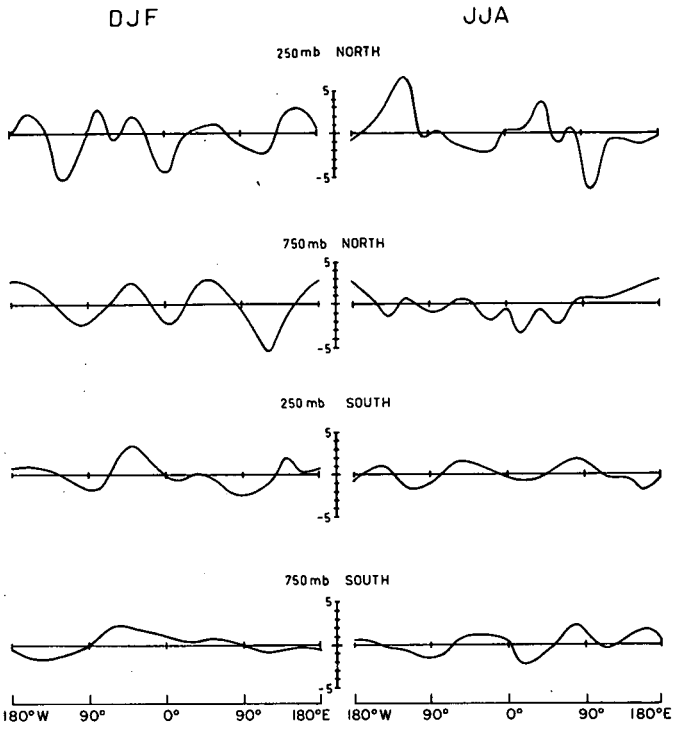

FIGURE 2.—Lateral boundary conditions for the two seasons, DJF and JJA, shown as a function of longitude at the 250- and 750-mb levels in each hemisphere. Curves are of the time-averaged meridional velocity component, v (in m/s), extracted from Kidson (1968).

$$v_i(\mu,\varphi)=\mathrm{Rl}\sum_s v_{i,s}(\mu)\exp(is\varphi) \tag{4}$$

where s is an integer and Rl signifies the real part of the expansion. Formulation in the two-layer system and the use of eq (4) yield a set of seven equations in μ-dependent, complex, Fourier coefficients. The equations are then expressed in finite-difference form between the lateral boundaries of the Tropics. In an identical manner to that described in W1, the resulting seven, first-order, difference equations are reduced to a pair of linear, coupled and complex, second-order, difference equations in $v_{1,s}$ and $v_{2,s}$. These are expressed at each gridpoint, k, in the μ domain; that is,

$$p_1^k v_1^{k+1}+p_2^k v_1^k+p_3^k v_1^{k-1}+p_4^k v_2^{k+1}+p_5^k v_2^k+p_6^k v_2^{k-1}=0$$
and
$$q_1^k v_1^{k+1}+q_2^k v_1^k+q_3^k v_1^{k-1}+q_4^k v_2^{k+1}+q_5^k v_2^k+q_6^k v_2^{k-1}=0 \tag{5}$$

where the p_1^k and q_1^k are complex functions of the coefficients of eq (2). The subscript s is understood.

Twenty-seven gridpoints were used between the latitudinal boundaries. The meridional velocities at the boundaries are supplied as known functions (Mak 1969), and eq (5) is expressed in matrix form. Inversion of the matrix provides the response of the Tropics to an imposed lateral forcing.

3. THE LATERAL BOUNDARY CONDITIONS

The lateral conditions on the equatorial channel were compiled using data from Kidson (1968) and are shown in figure 2. These represent the seasonally averaged meridional velocity components at $\mu=\pm0.65$ (approx. 40°N and 40°S) for DJF and JJA.

It is important to know whether or not the fields of figure 2 represent a flux of wave energy from high to low latitudes, thereby ensuring that it is the midlatitudes that are doing work on the Tropics. This occurs if the perturbation meridional velocity correlates negatively with the perturbation geopotential in the Northern Hemisphere or positively in the Southern Hemisphere. Unfortunately, few estimates of the wave energy flux appear to exist, especially for south of the Equator, and one is forced to consider an indirect method of determination of the flux using a more readily available quantity. Such a quantity is the momentum flux across a latitude circle. Using midlatitude, quasi-geostrophic arguments, Eliassen and Palm [1961, eq (10.11)] relate the two quantities as

$$\overline{\Psi v}=-\bar{U}\overline{uv}, \tag{6}$$

which indicates that the flux of wave energy is in an opposite sense to the momentum flux if the basic flow is westerly.

Estimates of the momentum flux from 40°N to 30°S are given by Kidson et al. (1969). For both DJF and JJA, the momentum flux in the Northern Hemisphere due to the standing eddies is positive (see the $\overline{u}^*\overline{v}^*$ curve in their fig. 6) so that eq (6) infers a wave energy flux into the Tropics. Because of the extremely poor data coverage over the southern oceans, Kidson et al. (1969) do not extend their analyses poleward of 30°S. At this latitude, however, they estimate a small northward flux of momen-

tum in JJA and a near-zero flux in DJF. In another study, Obasi (1963) found a weak equatorward momentum flux during the Southern Hemisphere summer and an equally weak poleward momentum flux during the winter. From these two studies, it is apparent that the sense of the Southern Hemisphere standing eddy momentum flux is undefinable in the data-sparse south, especially since the data sources that do exist come from three narrow longitude bands (i.e., South America, South Africa, and Australia). On the other hand, the momentum flux due to the transient eddies at both boundaries of the equatorial channel are strongly poleward, which signifies that the net effect of the transient eddies in both midlatitudes is to produce an equatorial wave energy flux.

In the following sections, we will consider the response of the equatorial channel to the boundary conditions discussed in the preceding paragraphs. Before doing that, however, we will study the response of various basic fields to a simple hypothetical boundary condition imposed at the southern limits of the model Tropics. The form of the condition is

$$v_i(\mu=-0.6)=A_i \exp \frac{-81(\varphi-\pi)^2}{4\pi^2} \qquad (7)$$

where A_i is an arbitrary amplitude. The function represents a Gaussian-type curve which e-folds within $\pm 40°$ of longitude about the prime meridian.

4. RESPONSE OF THE EQUATORIAL CHANNEL

Zero-frequency or stationary modes, by virtue of their zero phase speed, will possess critical latitudes wherever the sign of the basic flow changes. An example of this is given in figure 3, where the Doppler-shifted frequencies are given by

$$\lambda_{DS}=-\frac{\overline{U}s}{a\Omega \sin\theta} \qquad (8)$$

and are plotted as a function of latitude. The basic flow is that defined by case T2 in table 1. T2 represents a barotropic basic current in which $\overline{U}_1 = \overline{U}_2$. The following points should be noted:

1. Poleward of $\mu=\pm 0.2$, only those modes with $\lambda<0$ are quasi-resonant. These correspond to the planetary-scale Rossby waves.
2. Equatorward of $\mu=\pm 0.2$, only the eastward propagation modes may be excited (Kelvin and eastward propagating gravity waves).
3. At $\mu=\pm 0.2$, a critical latitude exists for all zero-frequency or stationary waves. This corresponds to the latitude where the basic field of case T2 passes through zero. At these points, the zero phase velocity of *all* the stationary modes is exactly matched by the basic flow.

Thus, any stationary mode excited poleward of the μ_c should have little, if any, influence at very low latitudes. Similarly, modes that result from forcing within the easterly regime should not propagate poleward of the critical latitude (note fig. 9 of W1, which shows the response of the model to a hypothetical heat source placed at the Equator. Although the basic field corresponds to case T1, which is somewhat more complicated than is T2 because it includes vertical shear, we can see that the majority of the response is confined to a narrow belt within the easterlies).

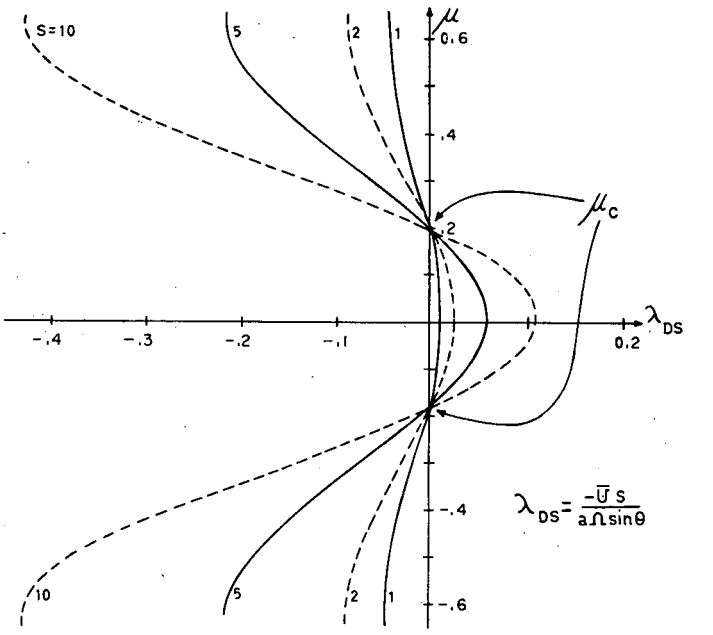

FIGURE 3.—The Doppler-shifted frequencies, λ_{DS}, of the (quasi-) resonant modes for the barotropic basic field, T2 (table 1). Note that all stationary modes are resonant at $\mu=\mu_c$ or where the basic zonal flow, T2, passes through zero.

Hypothetical Cases

The various hypothetical cases considered in this subsection are summarized in table 1. The basic field used in case T1 is identical to the basic field used in W1 to study the response of the Tropics to hypothetical forcing functions placed at low altitudes. Besides having the property of symmetry about the Equator, it is also a fair approximation to the mean of the DJF and JJA basic fields. In summary, the four cases represent the response of four basic fields within the equatorial channel to the identical forcing field [eq (7)] at the southern boundary. The four basic fields are characterized by both vertical and horizontal shear (T1), horizontal shear (T2), a constant eastward flow (T3), and a constant westward flow (T4). All fields are symmetric about the Equator. It is the purpose of this subsection to isolate the response of various simple tropical atmospheres to more readily understand the response of the complicated basic fields DJF and JJA.

Figures 4–7 indicate the response of the basic fields, T1–T4, respectively, to the specified hypothetical forcing. In the uppermost diagram of each figure (i.e., figs. 4A, 5A, 6A, 7A), the particular basic field is plotted as a function of latitude. Statistics of the particular response; namely, the kinetic energy, the momentum flux, and the wave energy flux in each layer, are shown in diagrams B and C of each figure.

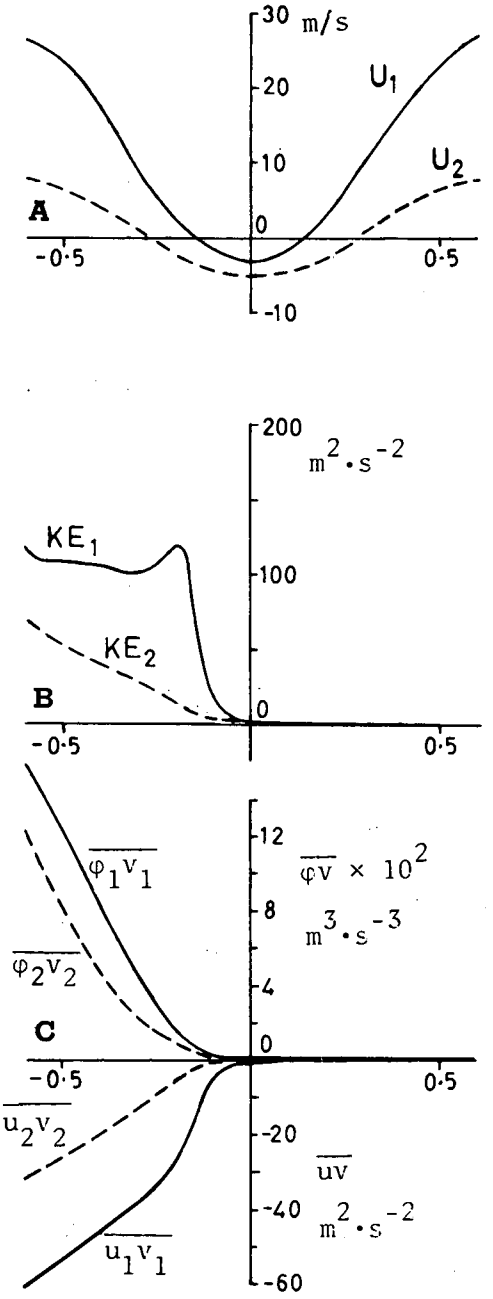

FIGURE 4.—(A) response of the basic field T1 of table 1 to the forcing specified by eq (7) at the southern boundary, (B) the zonally averaged kinetic energy in each layer ($\overline{KE_i}$), and (C) the zonal averages of the wave energy flux ($\overline{\phi_i v_i}$) and the momentum flux ($\overline{u_i v_i}$). Note the different scales on the ordinate for the momentum and wave energy flux. The fields are plotted as a function of the sine of latitude.

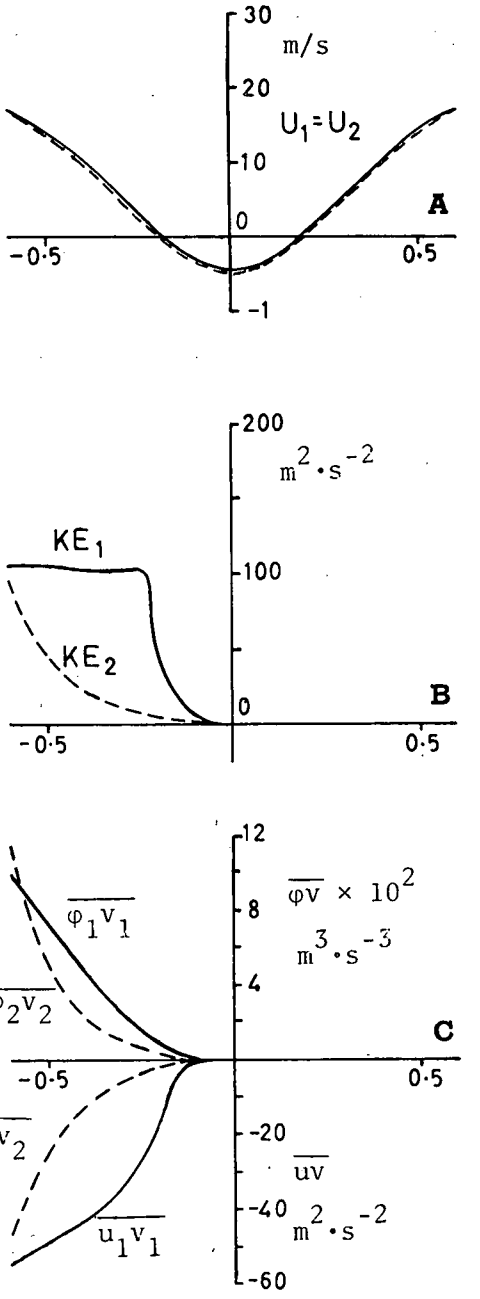

FIGURE 5.—Same as figure 4 for basic field T2 of table 1.

The response of T1 and T2 are similar although the magnitude of the former response is larger. This is not surprising, as the basic field, T2, is the mean of 250- and 750-mb parts of T1 (i.e., the "barotropic part" of T1). Both cases show a relatively sharp cutoff in response near the critical latitudes and both have negligible effect at very low latitudes. Similarly, both show a larger response in the upper layer of the model due principally to the smaller dissipation in the upper troposphere of the model. One apparent difference is that the cutoff of T1 is equatorward of T2. Presumably, this is due to T1 possessing two critical latitudes, one in the upper layer and one in the lower. Since the largest response occurs in the upper layer, it is that critical latitude being closer to the Equator than the critical latitude in T2 that would be the more important limit of energy propagation.

One further common feature of cases T1 and T2 is that the cutoff of the response at the critical latitude is not abrupt but decreases rapidly in an exponential manner toward the Equator. We will discuss this phenomenon later. Cases T3 and T4 are shown in figures 6 and 7, respectively; they consider the response of two basic fields possessing neither vertical nor horizontal shear but constant eastward and westward flow. Consequently, neither possesses a critical latitute since $\overline{U}$ contains no zeros. Considering T3 first, we note that energy has propagated across the Equator and into the Northern Hemi-

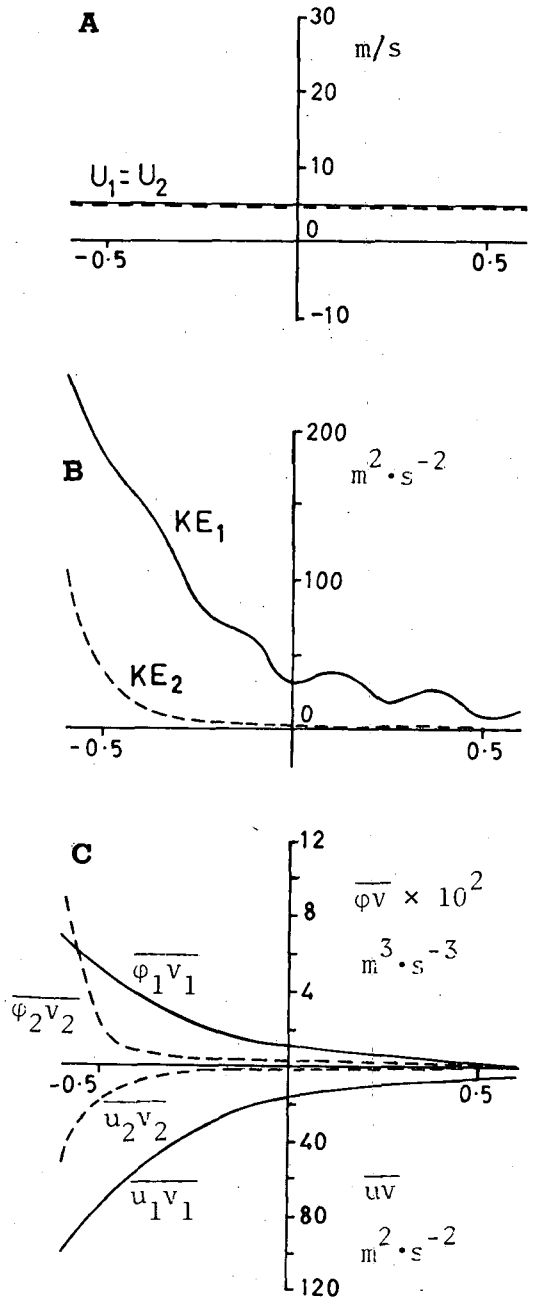

FIGURE 6.—Same as figure 4 for basic field T3 of table 1.

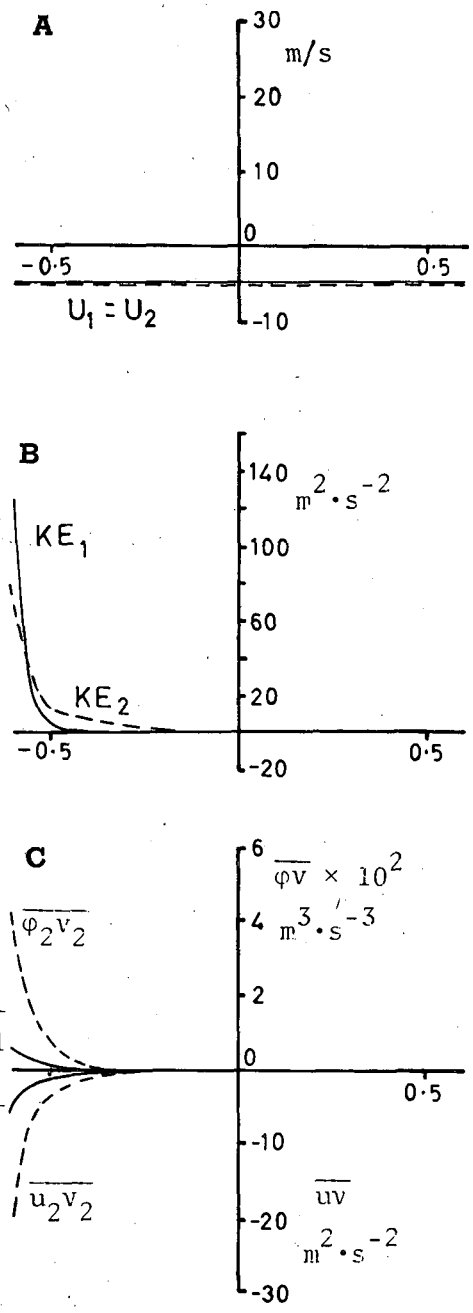

FIGURE 7.—Same as figure 4 for basic field T4 of table 1. Note that the ordinate scale has been increased.

sphere with the amplitude decreasing northward due to dissipation. Such a basic flow provides $\lambda_{DS} \approx -0.01s$. From Longuet-Higgins (1968), we see that, for small to moderate s, a whole range of planetary-scale, class 2 waves (Rossby waves) may be excited. (See app. B, W1 where similar interpretations of Longuet-Higgins' results are made.) For small s, the waves are confined near the Equator, but, as s increases (and so λ_{DS}), there exists the opportunity to excite waves closer to the boundaries of the model. The response of the purely westward current, T4, indicates almost zero effect over the whole equatorial channel except for a small effect near the forcing boundary. The response of both T3 and T4 may be explained using the arguments of Bennett and Young (1971).

For the shallow fluid analogy to our model, Bennett and Young derived the governing equation [their eq (21)] in the Fourier coefficient of the meridional velocity component, v, which is, in our notation,

$$v_{\mu\mu} + Q\left(s, \overline{U}, \frac{\lambda}{s}, \mu\right) v = 0. \tag{9}$$

This equation was obtained by scaling the equatorial β-plane equations relative to characteristics of planetary-scale tropical flow. The coefficient Q is given by

$$Q = -s^2 - \mu^2 + \frac{1 - \frac{d^2\overline{U}}{d\mu^2} + \mu^2\overline{U}}{\overline{U} - \frac{\lambda}{s}}, \tag{10}$$

which, for stationary or steady-state modes, becomes infinitely large as $U \to 0$. For $Q > 0$, eq (9) possesses oscillatory and propagating solutions and corresponds to case T3; whereas for $Q < 0$, it exhibits evanescent or exponentially decaying solutions. In the steady-state case, the sign of Q is nearly completely determined by the sign of U (at least for a physically realistic range of U) so that case T4 is correctly characterized by solutions that decay equatorward from the boundary.

The most obvious effect of dissipation can be seen in the relative magnitudes of the response in the two layers of the model. For example, in cases T1, T2, and T3, the response in the upper layer is much greater than that in the lower. This is due to the presence of the surface friction effect in the lower level (decay rate 6 days); whereas in the upper troposphere of the model, only the radiational cooling (40 days) and the vertical exchange of momentum due to small-scale processes (25 days) affect the response.

More subtle effects of dissipation may also be observed. As we have previously noted in cases T1 and T2, the response neither increases beyond bound nor goes to zero abruptly at the latitude where the basic flow passes through zero. Both of these effects are probably due to dissipation since a true critical latitude cannot exist in a dissipative system. This can be seen by using eq (10). In the zero-frequency case ($\lambda = 0$) with a nonzero basic flow, the denominator $\overline{U} - \lambda/s$ will be replaced by the Doppler-shifted frequency, λ_{DS}. With no dissipation, this is defined dimensionally by eq (8), which allows an infinite Q when $\overline{U} = 0$. However, in a dissipative system, the Doppler-shifted frequency may be defined to include the dissipation constant. That is,

$$\lambda_{DS} = -\left(\frac{\overline{U}_s}{a\Omega \sin\theta} + ik\right) \tag{11}$$

where k is some dissipative constant. This means that λ_{DS} is now complex, with the dissipation representing the imaginary part. Thus for any $\overline{U}$, λ_{DS} may never be zero and the response at the critical latitude will be finite. Furthermore, this means that energy may "seep" past the point where $\overline{U} = 0$ but in so doing enters the region where $\overline{U} < 0$, which requires evanescent solutions so that the response decays exponentially on the equatorward side of the critical latitude in a fashion similar to that observed in case T4. This also explains why in W1, when the Tropics were forced locally *within* the easterlies, small oscillations were apparent poleward of $\overline{U} = 0$.

The Seasonal Response

Figure 8 shows the seasonal basic fields for both DJF and JJA compiled from the data of Kidson (1968). From our interpretation of the hypothetical cases, we can expect the influence of the midlatitude forcing to penetrate very close to the Equator from the Northern Hemisphere in DJF and from the Southern Hemisphere in JJA. This is apparent from the zeros of the basic field in the upper layer in both seasons. The magnitude of the low-latitude

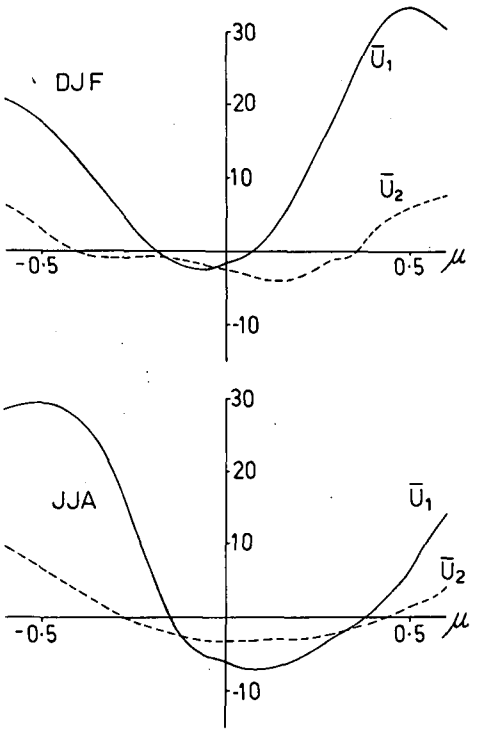

FIGURE 8.—The basic zonal wind, $\overline{U}_1$ (250 mb), and $\overline{U}_2$ (750 mb), plotted as a function of the sine of latitude for DJF and JJA. Units are m/s.

response will depend upon the magnitude of the wave energy flux at the respective boundaries as well as the sign and magnitude of the basic field.

The latitudinal distribution of the zonally and vertically averaged perturbation kinetic energy is shown as the solid line in figure 9 (labeled R). As anticipated in the preceding paragraph, the effect of the midlatitudes in the winter hemisphere reaches very close to the Equator. The magnitudes at low latitudes are much greater in DJF, but this is consistent with the larger magnitudes of the forcing functions as indicated by figure 2. In JJA, a fairly abrupt cutoff in the response occurs in the vicinity of the zeros of the basic field near $\mu = 0.4$ with the characteristic exponential decay equatorward of the critical latitude (cf. T2 and T3).

Figure 10 shows the perturbation horizontal velocity and height fields at 750 and 250 mb due to forcing of the DJF basic field (fig. 8) with the appropriate set of boundary conditions shown in figure 2. The equivalent JJA response is shown in figure 11. The units of the height field are meters and the scale of the velocity vector is indicated by the legend on each figure. The figures indicate that the response for both seasons consists of a series of troughs and ridges associated with the sign of the flux in the longitude region 180°–90°W at 250 mb in DJF. Figure 2 shows that in the Northern Hemisphere this longitude zone has a northerly velocity component in the west and a southerly component in the east (i.e., approx. 135°–90°W). Figure 10 indicates that this corresponds to a strong ridge system tilted from the southwest to the northeast. The apparent deflection of the boundary flux given by the boundary conditions is consistent with the sign of the Coriolis force in the appropriate hemisphere.

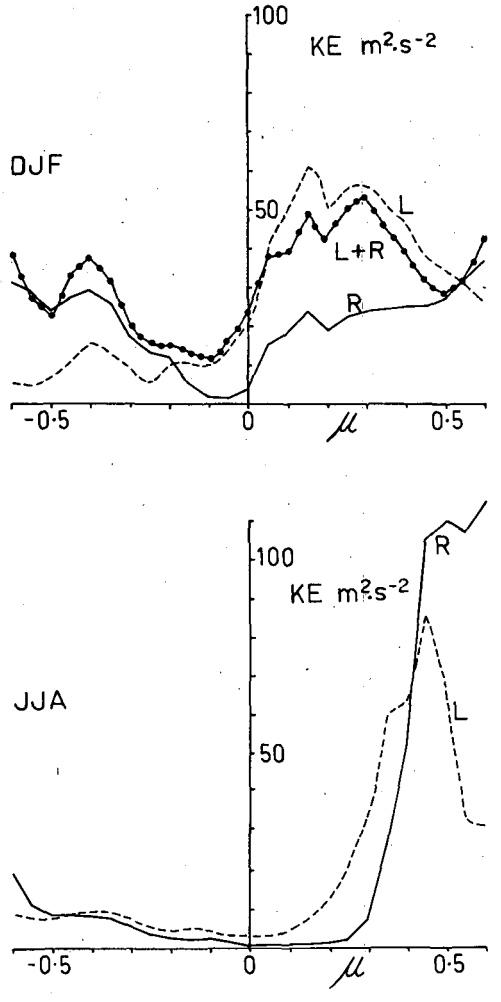

FIGURE 9.—Latitudinal distribution of the zonally and vertically averaged perturbation kinetic energy that results from local forcing, L, and remote forcing, R, of the two seasons DJF and JJA. The kinetic energy field resulting from a combination of the forcing is plotted on the DJF diagram.

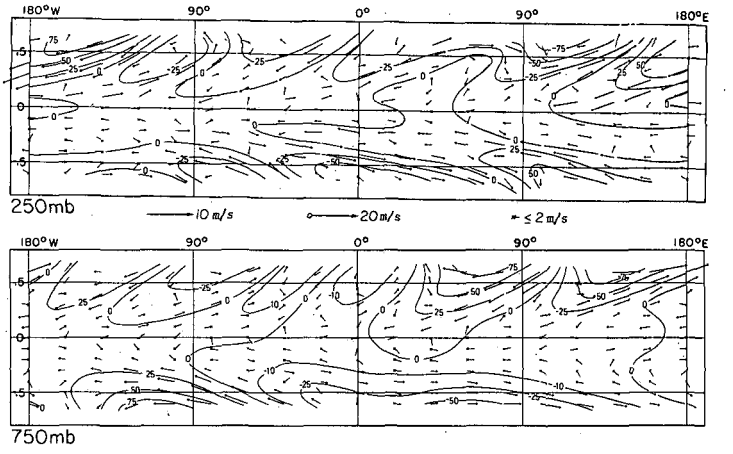

FIGURE 10.—Horizontal perturbation velocity response (vectors) and geopotential height deviations (solid lines) of the DJF basic field at 250 and 750 mb to the appropriate seasonal forcing shown in figure 2. The vector magnitude is proportional to the indicated scale except that all vectors of magnitude less than 2 m/s are of the same length and emanate from a cross.

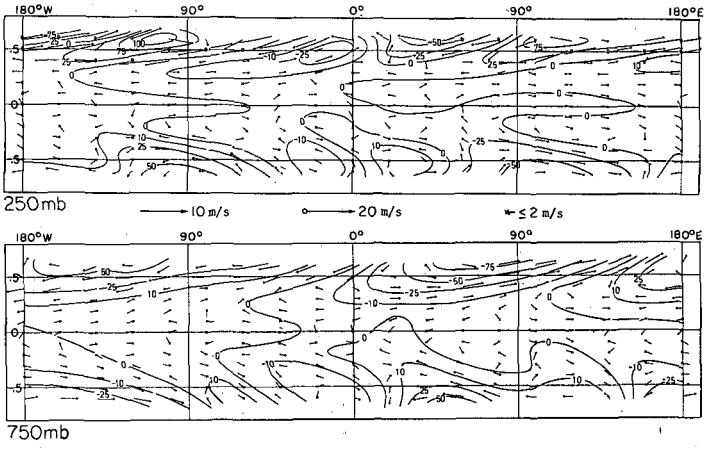

FIGURE 11.—Same as figure 10 for JJA.

The resultant tilt of the troughs corresponds to a poleward flux of momentum and, from eq (6), an equatorial wave energy flux. Near the boundaries of the equatorial channel, the velocity vectors are almost parallel to the isopleths of geopotential. This near-geostrophy decreases toward the Equator so that at very low latitudes the velocity vectors are parallel to the geopotential gradient.

In the next section, we will compare this low-latitude response resulting from midlatitude effects with the perturbation fields generated by localized low-latitude forcing functions and finally compare the sum of these responses with the observed mean perturbation state of the tropical atmosphere.

5. COMPARISON OF LOCAL AND REMOTE FORCING

To compare the results presented in this paper with those given in W1, we must ensure that the two models are equivalent. As previously mentioned, the only difference between the two models is the addition of lateral boundaries at $\mu = \pm 0.65$, thus reducing the domain from a full sphere to an equatorial channel. To test the equivalence, we used the same heating and orographic functions to drive the bounded model as were used to drive the full spherical model in W1. Only one change was made. In the spherical model, the forcing functions were allowed to decay exponentially poleward of $|\mu| = 0.5$. In the bounded model, an identical decay was allowed except that the functions were set to zero at the boundaries (i.e., $|\mu| = 0.65$). The magnitude of the difference between the models decreased from about 7 percent in the kinetic energy at $\mu = 0.6$ to zero near the Equator. With this near-equivalence of the two models in mind, a comparison of the two forms of forcing appears allowable. Furthermore, the total response (i.e., that resulting from both remote and local forcing) may be compiled from the sum of the two separate responses due to the linear properties of the model. The energetics of the total response were formed from these fields.

The dashed curves on figure 9 represent the latitudinal distribution of the zonally and vertically averaged kinetic energy due to local forcing taken from W1. Comparing this with the kinetic energy due to remote forcing, we find that the relative magnitudes of the two distributions vary both as a function of latitude and season. For example, in the Southern Hemisphere summer, the effect

TABLE 2.—*Ratio of the zonally and vertically averaged perturbation kinetic energy fields (i.e., KE_R/KE_L) as a function of latitude resulting from remote (R) and local (L) forcing. The response to local forcing is calculated in W1.*

μ	−0.6	−0.5	−0.4	−0.3	−0.2	−0.1	0.0	0.1	0.2	0.3	0.4	0.5	0.6
DJF	6.9	4.0	1.9	1.9	1.2	.17	.18	.38	.4	.42	.56	.82	1.8
JJA	2.3	1.2	0.97	0.64	0.48	.57	.2	.12	.12	.2	.85	2.0	4.5

of remote forcing is greater than the local forcing poleward of $\mu=-0.2$; whereas, in JJA, the two effects are approximately equal. The ratio of the two kinetic energy distributions is shown in table 2. In summary, we find that in DJF the effect of the local forcing functions outweighs the remote effect in the range $-0.2<\mu<0.55$ and, in JJA, in the range $-0.45<\mu<0.45$. The curve labeled (L+R) is the DJF kinetic energy distribution resulting from the combined local and remote forcing. Note that the R and L effects are not additive (the kinetic energy of the combined forcing is calculated from the sum of the individual velocity fields due to remote and local forcing) and that the introduction of remote forcing appears to reduce the kinetic energy of the response resulting from local forcing in the Northern Hemisphere but increases it in the Southern Hemisphere.

Figures 12 and 14 show the perturbation velocity and geopotential fields due to the combination of remote and local forcing for DJF and JJA, respectively. These fields were calculated as the linear sums of the response due to local forcing (W1) and remote forcing. The observed perturbation velocity fields for the corresponding seasons, but for the 700- and 300-mb levels, are shown in figures 13 and 15. In making comparisons between the computed and observed fields, one should remember the scarcity and grouping of the data points in the Southern Hemisphere. Since the fields shown in figures 13 and 15 are perturbation quantities, they are especially sensitive to the density of the data network. For example, an error in the zonally averaged velocity may result in a perturbation quantity of the wrong sign.

Although the velocity fields are far from perfect, they do appear to be improvements on the fields produced by merely local forcing. This is especially true in the subtropics, where the largest deviations between the locally forced Tropics and the observed Tropics were found in W1. For example, there is much closer approximation between the flow in both the upper and lower troposphere over the Pacific Ocean during DJF. Both the observed and computed upper level fields indicate a cyclonic circulation just north of the Equator and a ridge to the north, and both fields also possess a broad westerly belt extending across the Equator into the Southern Hemisphere. In the Eastern Hemisphere, most of the large-scale observed features appear to be predicted, although the model still tends to overestimate the effect of the Himalayan Mountains. (See W1 for a discussion of this point.) Areas of considerable difference still exist, however. For example, in the lower troposphere of the DJF fields, the direction of flow over north Africa and the western Indian Ocean is opposite that of the observed perturbations.

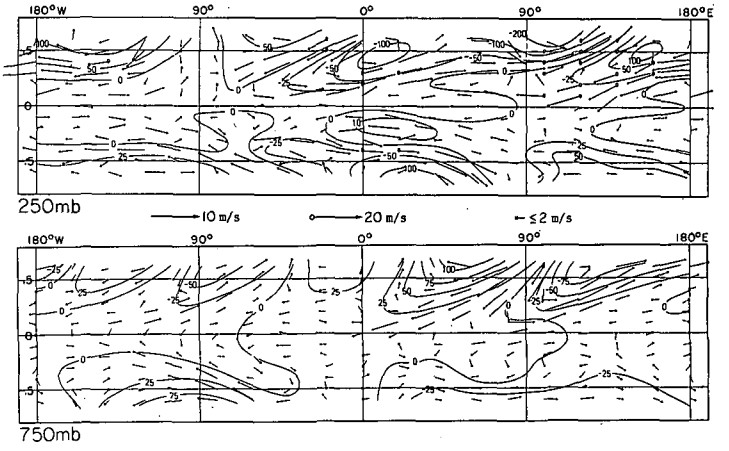

FIGURE 12.—Same as figure 10 for a combination of local and remote forcing of the DJF basic field.

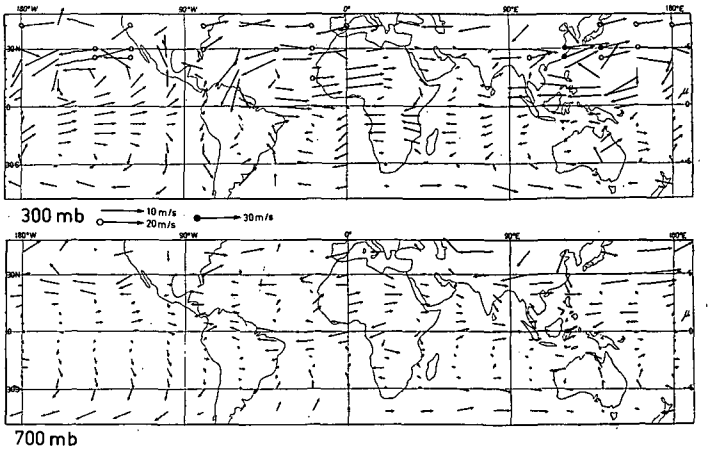

FIGURE 13.—Observed horizontal perturbation velocity field for DJF at 700 and 300 mb (data from Newell et al. 1972). Vector format is the same as in figure 10 except that magnitudes of less than 2 m/s receive no special treatment.

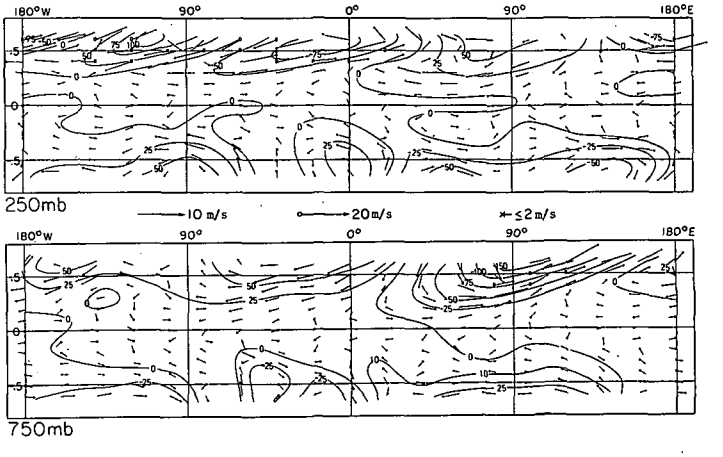

FIGURE 14.—Same as figure 10 for a combination of local and remote forcing of the JJA basic field.

The greatest differences between the observed flow and that produced by local forcing occurred in the north Pacific Ocean during JJA. With remote effects included, the situation is improved but still unsatisfactory as can be seen by comparing figures 14 and 15. The trough–ridge system in the upper troposphere appears to be predicted rather far to the west of its observed position. Except for this feature, most of the gross characteristics of the JJA

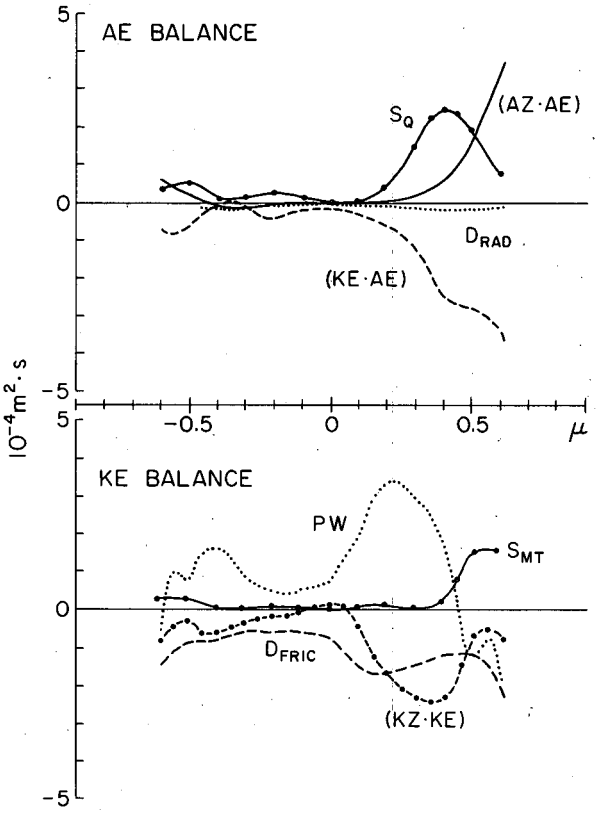

FIGURE 15.—Same as figure 13 for the observed JJA field.

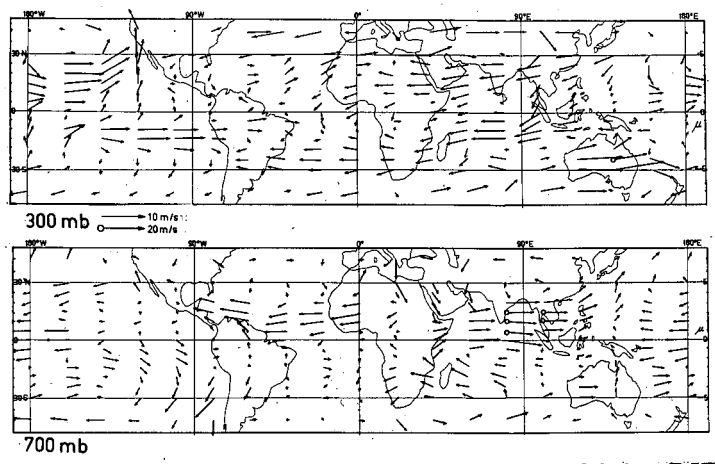

FIGURE 16.—Energy balance of the two-layer model for DJF due to combined remote and local forcing. The various processes are labeled in the notation of eq (12) and (13). For clarity, the (AE·KE) curve is shown only with the AE balance.

flow at both levels appear approximately simulated in both magnitude and direction. In W1, the predicted easterly jet stream over the Indian Ocean was stronger than observed; while, with forcing at the boundaries, the magnitudes of the two estimates are closer. A comparison of the flow over the continental regions of the Southern Hemisphere indicates some agreement, but over the southern oceanic regions the estimates differ. For example, while both estimates allow anticyclonic circulations just south of the Equator in the central Pacific, the agreement decreases to the south; because of the scarcity of data in this region, it is difficult to know whether the fault lies with the model or with the observations. Even the more recent observational study by Krishnamurti (1971), in which the conventional data is supplemented with aircraft observations, fails to help in these regions.

The latitudinal distributions of the zonally and vertically averaged available potential and kinetic energies (AE and KE) for DJF are shown in figure 16. These were calculated using the summed response of the local and remote forcing. The KE and AE budget equations for a steady-state atmosphere may be written in schematic form as

$$(\mathrm{KZ}\cdot\mathrm{KE})+(\mathrm{AE}\cdot\mathrm{KE})+\mathrm{PW}+\mathrm{D_{FRIC}}=\mathrm{S_{MT}} \qquad (12)$$

and

$$(\mathrm{AZ}\cdot\mathrm{AE})+(\mathrm{KE}\cdot\mathrm{AE})+\mathrm{D_{RAD}}=\mathrm{S_Q} \qquad (13)$$

where $(x\cdot y)$ refers to an energy conversion from form x to form y. AZ and KZ refer to the available potential and kinetic energies of the mean zonal flow, respectively.

Using eq (2), we may write the terms of eq (12) and (13) as

$$(\mathrm{KZ}\cdot\mathrm{KE})=(\Delta_1-\Delta_2)[\omega(u_1+u_2)+\omega(p=p_0)u_2]-(\Delta_{1y}[u_1v_1]+\Delta_{2y}[u_2v_2]),$$

$$(\mathrm{AE}\cdot\mathrm{KE})=-2[\omega(\psi_1-\psi_2)],$$

$$\mathrm{PW}=-([v_1\psi_1]+[v_2\psi_2])_{y'},$$

$$(\mathrm{AZ}\cdot\mathrm{AE})=\frac{(\Delta_1-\Delta_2)(1+\Delta_1+\Delta_2)\mu[(v_1+v_2)(\psi_1-\psi_2)]}{2\bar{S}},$$

$$\mathrm{S_{MT}}=[\psi\omega_G],$$

$$\mathrm{S_Q}=[(\psi_1-\psi_2)Q(\mu,\varphi)],$$

$$\mathrm{D_{FRIC}}=\frac{2\{K_1([u_1u_2]+[v_1v_2])-(K_2[\mathrm{KE_1}+\mathrm{KE_2}])\}}{1-\mu^2},$$

and

$$\mathrm{D_{RAD}}=-K_3[\mathrm{AE}]$$

where

$$[\ \ ]=\frac{1}{2\pi}\int_0^{2\pi}d\varphi,$$

$$\mathrm{KE}_i=\frac{(u_i^2+v_i^2)}{2},$$

and

$$\mathrm{AE}=\frac{(\psi_1-\psi_2)^2}{2\bar{S}}.$$

K_1, K_2, and K_3 refer, respectively, to coefficients of surface drag, small-scale momentum exchange, and radiational cooling.

In addition to the conversion of energy from one form to another, eq (12) and (13) show that the AE can increase by external heating ($S_Q>0$), while the KE may increase by the interaction of orography with the basic flow ($S_{MT}>0$) and by work being done on the system via the pressure work term, PW. A full account and derivation of eq (12) and (13) from eq (2) is given in W1.

The characteristics of the energy distributions (fig. 16) are similar to those shown in W1 for the local forcing, especially in the AE equation. The main differences occur in the KE equation through which the midlatitude effect enters via the PW term. The major changes in this budget occur in the subtropics and in the magnitude of the PW term in the Southern Hemisphere. In W1, an extensive comparison was made between the KE budget of Manabe et al. (1970, fig. 6.1) and the energetics of the response due to local forcing. Whereas the energetics of this simple model including remote forcing are not identical to those of Manabe et al., the sense of the change of the distributions, especially in the Southern Hemisphere, is in the right direction.

6. CONCLUDING REMARKS

Within the confines of a simple, linear, two-layer model, the importance of extratropical forcing on the seasonal structure of the tropical atmosphere has been studied. To do this, we assumed that the total response of the tropical atmosphere is the linear sum of the effect of local forcing functions (W1) and remote forcing functions. A comparison of this "total" response with observational data indicated a significant improvement, especially in the subtropical regions, over the results of similar comparisons made using only the local response (W1).

The definition of the total response in the preceding paragraph details the basic simplicity of the model. It is surprising that, with a linear model, the circulation patterns are as similar as they appear to be. In the real atmosphere, many forms of self-interaction or feedback mechanisms are of obvious importance; interaction of convection and larger scale motion in the tropical atmosphere is one example. Also, it is not an easy task to strictly define the difference between local and remote forcing functions except, perhaps, with static functions such as orography. With heating effects in a moist atmosphere, it is much more difficult. In addition to the influence of local sensible fluxes of heat from an underlying surface prompting the release of latent heat, one has to consider the possibility of midlatitude forcing causing low-latitude convergence, the release of latent heat, and the generation of a whole class of disturbances. Unfortunately, our method of including the heating in the model (local forcing) cannot tell how the particular mean heating distribution came about, and, because we do not include a nonlinear hydrology cycle, we cannot calculate the amount of latent heat released due to remote forcing alone.

Because of the simplicity of the model and the relative crudeness in which the forcing functions and complicated feedback mechanisms of the atmosphere have been represented, one must be careful in the interpretation of the results. Although it is tempting to attribute the similarity of the results to a successful modeling of the dominating physics of the steady-state tropical atmosphere, it would be difficult to justify this further. However, it is the very simplicity of the model that has allowed us to study and test various physical processes and concepts that would have been beyond our reach with a more sophisticated nonlinear model. Therefore, an interpretation of atmospheric processes from the results of this model should be made within the confines of the simplicity of the model.

REFERENCES

Bennett, John R., and Young John A., "The Influence of Latitudinal Wind Shear Upon Large-Scale Wave Propagation Into the Tropics," *Monthly Weather Review*, Vol. 99, No. 3, Mar. **1971**, pp. 202–214.

Booker, John R., and Bretherton, Francis P., "The Critical Layer for Internal Gravity Waves in a Shear Flow," *Journal of Fluid Mechanics*, Vol. 27, Pt. 3, Cambridge University Press, England, Feb. 24, **1967**, pp. 513–539.

Charney, Jule G., "A Further Note on Large-Scale Motions in the Tropics," *Journal of the Atmospheric Sciences*, Vol. 26, No. 1, Jan. **1969**, pp. 182–185.

Dickinson, Robert E., "Development of a Rossby Wave Critical Level," *Journal of the Atmospheric Sciences*, Vol. 27, No. 4, July **1970**, pp. 627–633.

Eliassen, Arnt and Palm, Enok, "On the Transfer of Energy in Stationary Mountain Waves," *Geofysiske Publikasjoner*, Vol. 22, No. 3, Olso, Norway, Sept. **1961**, 23 pp.

Jones, Walter L., "Propagation of Internal Gravity Waves in Fluids With Shear Flow and Rotation," *Journal of Fluid Mechanics*, Vol. 30, Pt. 3, Cambridge University Press, England, Nov. 29, **1967**, pp. 439–448.

Kidson, John W., "The General Circulation of the Tropics," Ph. D. thesis, Department of Meteorology, Massachusetts Institute of Technology, Cambridge, Mass., Sept. **1968**, 205 pp.

Kidson, John W., Vincent, Dayton G., Newell, Reginald E., "Observational Studies of the General Circulation of the Tropics: Long Term Mean Values," *Quarterly Journal of the Royal Meterological Society*, Vol. 95, No. 404, London, England, Apr. **1969**, pp. 258–287.

Krishnamurti, T. N., "Observational Study of the Tropical Upper Tropospheric Motion Field During the Northern Hemisphere Summer," *Journal of Applied Meteorology*, Vol. 10, No. 6, Dec. **1971**, pp. 1066–1096.

Longuet-Higgins, M. S., "The Eigenfunctions of Laplace's Tidal Equations Over a Sphere," *Philosophical Transactions of the Royal Society of London*, Ser. A., Vol. 262, No. 1132, England, Feb. 29, **1968**, pp. 511–607.

Mak, Man-Kin, "Laterally Driven Stochastic Motions in the Tropics," *Journal of the Atmospheric Sciences*, Vol. 26, No. 1, Jan. **1969**, pp. 41–64.

Manabe, Syukuro, Holloway, J. Leith, Jr., and Stone, Hugh M., "Tropical Circulation in a Time-Integration of a Global Model of the Atmosphere," *Journal of the Atmospheric Sciences*, Vol. 27, No. 4, July **1970**, pp. 580–613.

Newell, Reginald E., Kidson, John W., Vincent, Dayton G., and Baer, George J., *The General Circulation of the Tropical Atmosphere and Interactions with Extratropical Latitudes*, MIT Press, Massachusetts Institute of Technology, Cambridge, **1972** (in press).

Obasi, G. O. Patrick, "Atmospheric Momentum and Energy Calculations for the Southern Hemisphere During the I.G.Y.," *Final Report, Scientific Report* No. 6, Contract No. AF 19(604)-6108, Planetary Circulation Project, Department of Meteorology, Massachusetts Institute of Technology, Cambridge, Mass., **1963**, 354 pp.

Rossby, Carl-Gustav, and others, "Relations Between Variations in the Intensity of the Zonal Circulation of the Atmosphere and the Displacements of the Semi-Permanent Centers of Action," *Journal of Marine Research*, Vol. 2, No. 1, **1939**, pp. 38–55.

Webster, Peter J., "The Response of the Tropical Atmosphere to Local, Steady Forcing," *Monthly Weather Review*, Vol. 100, No. 7, July **1972**, pp. 518–541.

[*Received March 7, 1972; revised October 27, 1972*]